IRAQI JOURNAL OF MATERIALS
Volume (2) Issue (4) October-December 2023, pp. 181-188

Effect of Lateral Shear Interferogram on Path Difference in Coherent Optical Systems

Olan Danatua, Ekroma Nadinza

Department of Physical Sciences, School of natural and Applied Sciences, Kampala International University, Kampala, UGANDA

Abstract
In this work, an analytical treatment for the wavefront propagation in optical systems is proposed. This treatment has taken into account the effects of lateral and radial shear interferograms between wavefronts as well as the order of the wavefront that depends on the incidence angle. Results showed that the wavefront ordinary and magnified deviations are convergent at low order rays while the high values of lateral shear can minimize the optical path difference between the propagating wavefronts.

Keywords: Shearing interferometer; Optical system; Interferogram; Path difference
Received: 18 April 2023; **Revised:** 26 July 2023; **Accepted:** 2 August 2023; **Published:** 1 October 2023

1. Introduction

In a shearing interferometer, both wavefronts are derived from the system under test, and the interference pattern is produced by shearing one wavefront with respect to the other [1]. Shearing interferometers have the advantage that they do not require a reference surface of the same dimensions as the system under test [2]. In addition, since both the interfering beams traverse very nearly the same optical path, the fringe pattern is less affected by mechanical disturbances [3].

To produce fringes of good visibility with a shearing interferometer, the beams must have adequate spatial coherence [4]. With thermal radiation, this requires a very small illuminated pinhole and, hence, an intense source, usually generating radiation with limited temporal coherence. As a result, much effort went into the design of shearing interferometers which were compensated for white light [5]. With the availability of lasers, which give light with a high degree of spatial and temporal coherence, many simpler arrangements have come into use [6].

The simplest type of shear is a lateral shear. With a nearly plane wavefront, this involves producing two images of the wavefront with a mutual lateral displacement, whereas with a nearly spherical wavefront it requires a similar displacement of the two images of the wavefront over the surface of the reference sphere [7]. Figure (2) shows three typical optical systems which can be used with converging wavefronts. These systems, which are based on the Michelson, Mach–Zehnder, and Sagnac interferometers, were described, respectively [8-10]. A number of modifications of these systems for use with spherical and plane wavefronts have been reviewed [11].

A particularly simple arrangement [12], which can be used with a laser source, consists of a plane-parallel plate. As shown in Fig. (3), the light from the laser is focused by a microscope objective on a pinhole located at the focus of the lens under test. The beam emerging from this lens gives rise to two wavefronts reflected from the front and back surfaces of the plate. The lateral shear between these wavefronts can be varied by tilting the plate and is given by the relation [13]:

$$s = \frac{d\ sin2\theta}{\sqrt{n^2 - sin^2\theta}} \qquad (1)$$

where d is the thickness of the plate and θ is the angle of incidence

A modification of this arrangement [14] uses two separate plates with a variable air gap. This has the advantage that a tilt can be introduced between the two sheared wavefronts to make the interpretation of the fringes easier. The use of a liquid-crystal phase retarder for phase-shifting has been described [15].

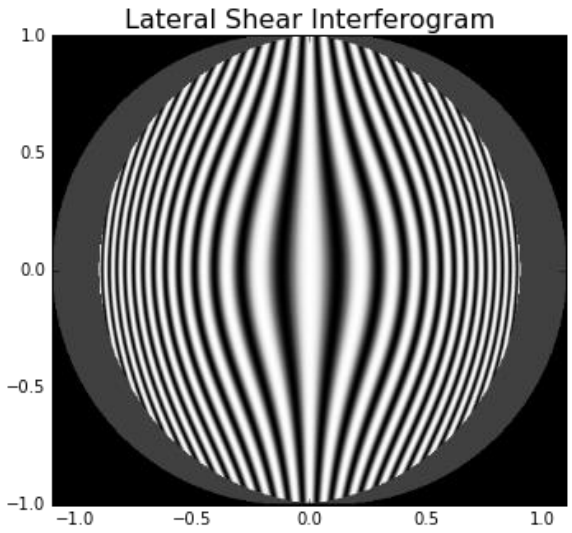

Fig. (1) Shear interferogram with 0.2 shearing

A vectorial shearing interferometer based on the Mach–Zehnder configuration, incorporating a pair of wedge prisms, has been described [16]. Variable shear and tilt can be implemented along any direction, permitting the number of fringes and their direction to be controlled.

A possibility that is being explored is the use of a neural network for rapidly identifying and evaluating the primary aberrations in an interferogram [17].

Other forms of shear besides a lateral shear are possible. One is rotational shear in which interference takes place between two images of the test wavefront, one of which is rotated with respect to the other [18,19]. Another is reversal shear [20,21]. Perhaps the most useful is radial shear, in which one of the images of the wavefront is contracted or expanded with respect to the other [22,23].

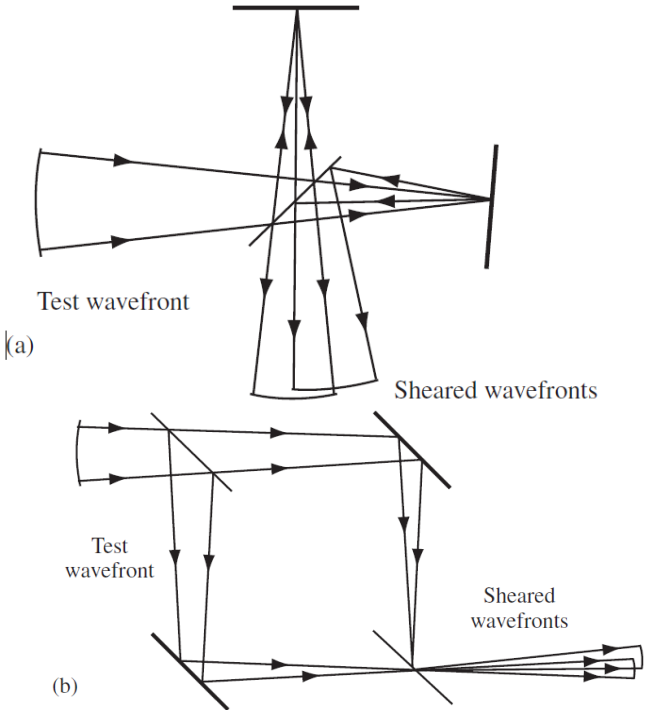

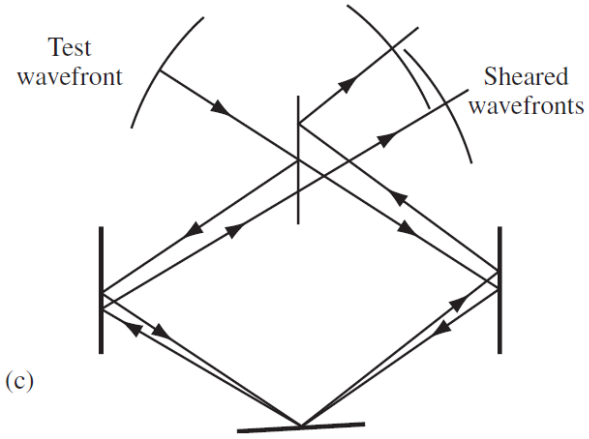

Fig. (2) Lateral shearing interferometers based on (a) the Michelson, (b) the Mach–Zehnder, and (c) the Sagnac interferometers

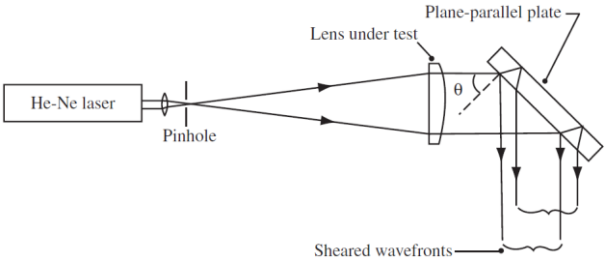

Fig. (3) Lateral shearing interferometer using a laser source and a tilted planeparallel plate [12]

2. Mathematical Treatment

A number of optical arrangements for radial shearing interferometers are available, which have been described [24]. With a thermal light source, a convenient arrangement uses a triangular path (Sagnac) interferometer in which two images of the test wavefront of different sizes are produced by a lens system which is traversed in opposite directions by the two beams [25]. With a laser source, a simple system can be used, consisting of a thick lens [26]. In this arrangement, interference takes place between the directly transmitted wavefront and the wavefront which has undergone one reflection at each surface. An even simpler system is shown in Fig. (4), in which interference takes place between the wavefronts reflected from two spherical surfaces [27,28]. A compact, in-line, radial shearing interferometer using a beamsplitting cube has been described [29]; one can also be set up with two zone plates [30,31].

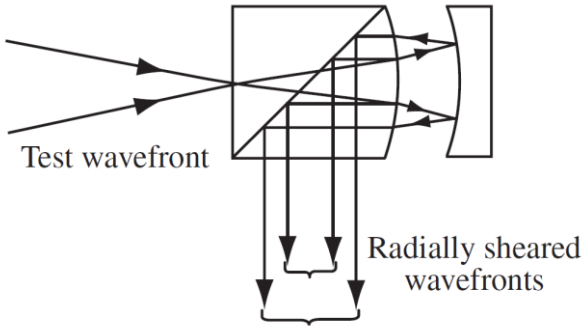

Fig. (4) Schematic diagram of the radial shear interferometer for use with a laser source [28]

To analyze a radial shearing interferogram it is convenient to express the deviations of the wavefront under test from a reference sphere in the form:

$$W(\rho,\theta) = \sum_{n=0}^{k}\sum_{l=0}^{n}\rho^{n}\,(A_{nl} + B_{nl}) \qquad (2)$$

ISSN (print) 2958-8960 (online) xxxx-xxxx Printed in IRAQ

where $A_{nl} = a_{nl}cos^{l}\theta$ and $B_{nl} = b_{nl}sin^{l}\theta$, ρ and θ are polar coordinates over a circle of unit radius defining the pupil

If the wavefront with which the test wavefront is compared is magnified by a factor (1/*S*), where *S*(<1) is known as the shear ratio, the deviations of this magnified wavefront from the same reference sphere are

$$W'(\rho,\theta) = \sum_{n=0}^{k}\sum_{l=0}^{n} S^{n}\rho^{n}(A_{nl} + B_{nl}) \qquad (3)$$

Accordingly, the optical path differences in the interferogram are given by the relation

$$p(\rho,\theta) = W(\rho,\theta) - W'(\rho,\theta)$$
$$p(\rho,\theta) = \sum_{n=0}^{k}\sum_{l=0}^{n}(1 - S^{n})\rho^{n}(A_{nl} + B_{nl}) \quad (4)$$

3. Results and Discussion

Figure (5) shows the variation of lateral shear of optical wavefront with the incidence angle for different values of order n. It is clear from Fig. (5a) that the fundamental wavefront (n=0) shows higher values of lateral shear and a maximum at the normal incidence (θ=0). The lateral shear is gradually decreasing to reach zero at the incidence angle of 90°. Therefore, the normal incidence is required for the situations of maximum lateral shear in contrast to the most experimental situations (n≥2) where the maximum lateral shear is located around 47°. As the order increases to more than 2, the maximum of lateral shear variation is shifted towards smaller angles. This is in good agreement with literature and published works.

For the case n=1, a completely different behavior is observed for the lateral shear with incidence angle, as shown in Fig. (5b). An apparent maximum is observed at an incidence angle of 38.38°, which makes the order n=1 looks like a singularity or ultra-narrow signal. This behavior is effectively invested in optical design of resonance cavities in laser design.

The interpretation of a lateral shearing interferogram is more difficult than that of an interferogram obtained with a Twyman–Green interferometer, since interference takes place between two aberrated wavefronts instead of between the aberrated wavefront and a perfect reference wavefront. The analysis of such an interferogram has been discussed [32,33]. Apolynomial $\Delta W(x,y)$ is fitted to the measured values of the optical path difference in two interferograms with mutually perpendicular directions of shear; the coefficients of $W(x,y)$ the polynomial representing the errors of the test wavefront, can then be derived from the coefficients of $\Delta W(x,y)$ [34-36]. Other approaches use Fourier filtering [37] or a least-squares method [38-40]. Alternatively, the differences obtained by shearing the test wavefront in a number of directions can be analyzed [41].

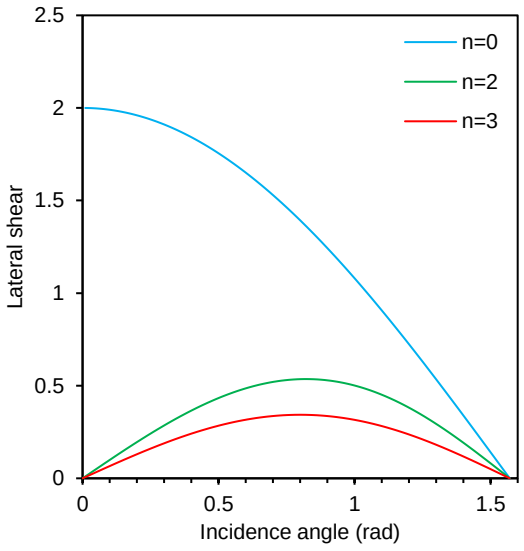

(a)

ISSN (print) 2958-8960 (online) xxxx-xxxx Printed in IRAQ

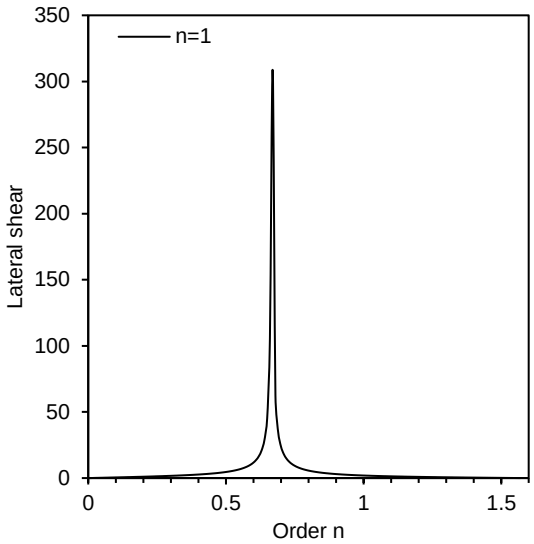

(b)

Fig. (5) Variation of lateral shear with incidence angle for three different values of order n

In order to introduce the behavior of wavefront deviation W(ρ,θ) as the order is varied, the wavefront deviation was plotted as a function of order (ℓ), as shown in Fig. (6a). Designing the optical system to work at order values smaller than 20 may exhibit low wavefront deviation, which is often required for high-quality optical systems such as single-mode lasers and narrow-band photodetection [42]. Consequently, avoiding the higher values of wavefront deviation is not always an option as some applications of optics may require high wavefront deviation on account of signal quality. Similarly, the wavefront magnified deviation W'(ρ,θ) shows similar behavior with the order n but with reasonably lower amplitude (about two orders of magnitude) as can be seen in Fig. (6b). This similarity can be considered as an advantage for the proposed model especially when being employed in laser design.

The optical path difference (p) can be represented in Fig. (7). It is logical that the behavior of p(ρ,θ) is similar to those of wavefront deviation W(ρ,θ) and wavefront magnified deviation W'(ρ,θ). So, this curve can be used to introduce the effect of lateral shear on the optical design. It is apparent from a comparison of Eq. (4) with Eq. (3) that, with a reasonably small value of the shear ratio (S<0.5), the radial shear interferogram is very similar to the interferogram that would be obtained with a Twyman–Green interferometer, and the wavefront aberrations can be computed in a very similar fashion [43,44].

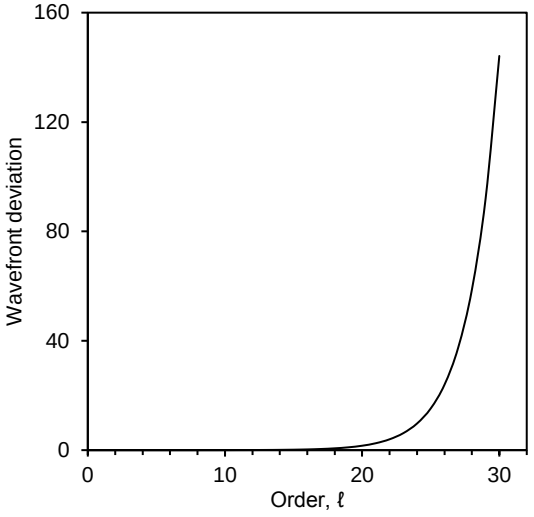

(a)

ISSN (print) 2958-8960 (online) xxxx-xxxx

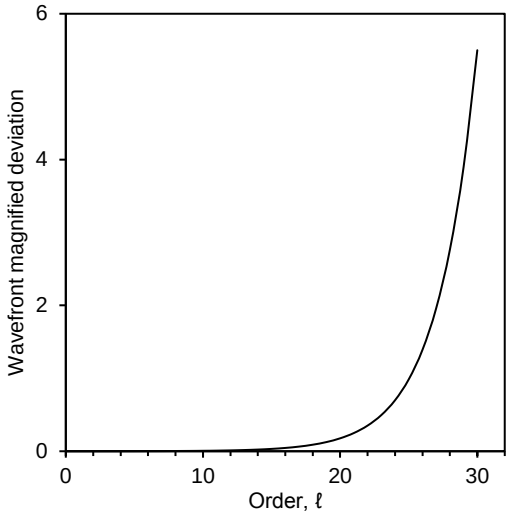

(b)

Fig. (6) Variation of wavefront deviation (a) and magnified deviation (b) with the order (ℓ) of light rays at incidence angle of 38.38°

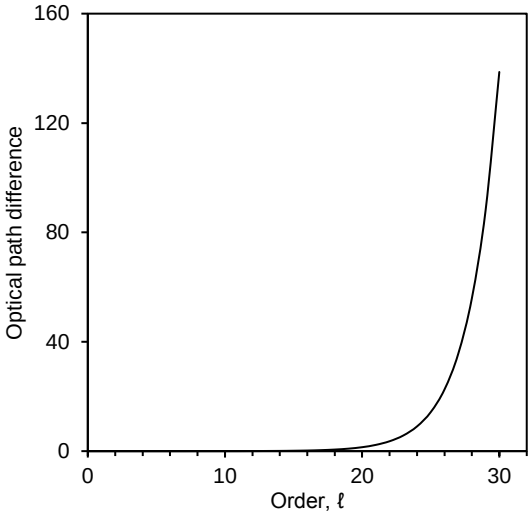

Fig. (7) Variation of optical path difference p(ρ,θ) with the order (ℓ) of light rays at incidence angle of 38.38°

The variation of optical path difference p(ρ,θ) with the order ℓ is shown in Fig. (8) for the wavefront deviation W(ρ,θ) and three different cases of the wavefront magnified deviation W'(ρ,θ) (S=0.2, 0.6 and 0.9). The low-order situation is apparently applicable as the optical path difference is ranging with 10^{-6}-10^{-4}. The high-order situation is highly dependent on the value of lateral shear between the propagating wavefronts to reach very low limits at orders of 30. Despite that the practical employments of such situation are rare, they still applicable. Amongst, unstable resonators of high-power lasers are examples.

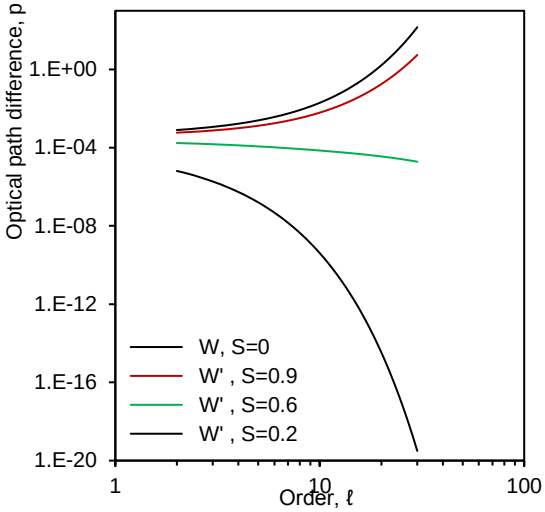

Fig. (8) Variation of optical path difference p(ρ,θ) with the order (ℓ) of light rays at incidence angle of 38.38° for different values of lateral shear s

4. Conclusion

In this work, an analytical treatment for the wavefront propagation in optical systems is proposed. This treatment has taken into account the effects of lateral and radial shear interferograms between wavefronts as well as the order of the wavefront that depends on the incidence angle. Results showed that the wavefront ordinary and magnified deviations are convergent at low order rays while the high values of lateral shear can minimize the optical path difference between the propagating wavefronts. Also, an optimum value of the incidence angle of 38.38° was determined for single-mode propagation, which is highly preferred in the optical systems employed in laser design.

References

[1] G. Xiong et al., “Interference pattern produced by shearing two wavefronts”, J. Opt. Design, 10(5) (2020) 367-372.
[2] Q. Wu et al., “Reference surface for shearing interferometers”, J. Opt. Technol., 13(3) (2017) 101-106.
[3] Y. Tian et al., “Effects of mechanical disturbances on fringe pattern formed by interfering beams”, Opt. Commun., 16(5) (2008) 283-287.
[4] J. Zhang et al., “Production of good-visible fringes with a shearing interferometer for spatial coherence applications”, J. Laser Technol., 9(7) (2008) 451-455.
[5] M.C. Obaiah et al., “Design of shearing interferometers for white light”, Opt. Phys. Lett., 18(1) (2020) 51-54.
[6] K. Bekeruglu et al., “Achievement of high degree of spatial and temporal coherence of laser”, Opt. Optoelect., 5(1) (2005) 89-93.
[7] Z. Li et al., “Image displacement of surface wavefront with reference sphere”, J. Opt. Phot., 10(4) (2020) 417-422.
[8] J. Huang et al., “Optical system with converging wavefronts based on Michelson interferometer”, Opt. Optoelect., 11(7) (2011) 691-698.
[9] A.H. Khan et al., “Optical system with converging wavefronts based on Mach–Zehnder interferometer”, J. Opt. Design, 9(4) (2019) 145-150.
[10] S. Kumar et al., “Optical system with converging wavefronts based on Sagnac interferometer”, J. Opt. Technol., 12(2) (2016) 99-104.
[11] J.H. White et al., “Modifications of optical systems for use with spherical and plane wavefronts”, Opt. Commun., 17(6) (2009) 375-380.
[12] C. Sun et al., “Simple arrangement of interferometer with plane-parallel plate laser source”, J. Laser Technol., 10(8) (2009) 555-560.
[13] O. Girma et al., “Calculation of lateral shear between propagating wavefronts”, Opt. Phys. Lett., 19(2) (2019) 163-168.
[14] H. Garg et al., “A modification of two-plate interferometer with variable air gap”, Opt. Optoelect., 6(2) (2006) 167-172.
[15] N. Ghahramani et al., “Use of liquid-crystal phase retarder for phase-shifting”, J. Opt. Phot., 9(3) (2019) 309-314.
[16] S. Xiang et al., “A vectorial shearing interferometer based on Mach–Zehnder configuration with wedge prisms”, Opt. Optoelect., 12(8) (2012) 725-730.
[17] L. Menini et al., “Using neural network for rapidly identification and evaluation of primary aberrations in interferograms”, J. Opt. Design, 8(1) (2018) 185-190.
[18] P. Kebria et al., “Rotational shear between two test wavefront”, J. Opt. Technol., 14(5) (2018) 305-310.
[19] L. Wang et al., “Analysis of rotational shear interferogram two images”, Opt. Commun., 18(1) (2010) 63-68.
[20] J. Qian et al., “Reversal shear interferometry”, J. Laser Technol., 11(9) (2010) 301-310.
[21] Y. Jiang et al., “Minimization of reversal shear in optical system based on interferometer”, Opt. Phys. Lett., 18(3) (2018) 301-308.
[22] A. Morshed et al., “Radial shear of relatively-moving visible signals”, Opt. Optoelect., 7(3) (2007) 221-226.
[23] A.A. Maciejewski et al., “Effects of radial shear on propagation of co-propagating wavefronts”, Opt. Optoelect., 8(4) (2008) 301-310.

[24] C Anderson et al., "Design considerations of high-efficiency radial shearing interferometer", J. Opt. Phot., 8(2) (2018) 201-206.
[25] G. Sellis et al., "Arrangement of Sagnac triangular path interferometer with thermal light source", J. Opt. Design, 7(7) (2017) 589-594.
[26] N. Katsikis et al., "A simple interferometer system using laser source and thick lens", J. Opt. Technol., 15(9) (2019) 1107-1112.
[27] S. Rakshit et al., "Analysis of interference between wavefronts reflected from two spherical surfaces", Opt. Commun., 19(4) (2011) 411-418.
[28] M. Kumbasar et al., "Spherical-surface reflection interferometer for propagating wavefronts", J. Laser Technol., 12(10) (2011) 691-700.
[29] M. Papadopoulos et al., "A compact, in-line, radial shearing interferometer using a beamsplitting cube", Opt. Phys. Lett., 17(4) (2017) 421-426.
[30] O.A. Hammadi and M.S. Edan, "Temperature Dependencies of Refractive Index and Optical Elasticity Coefficient on Lens Induced in Nd:YAG Crystal", Iraqi J. Appl. Phys., 8(1) (2012) 35-41.
[31] C. Pan et al., "Two-zone-plates radial shearing interferometer", J. Opt. Phot., 7(1) (2017) 21-26.
[32] C.-Y. Zu et al., "Analysis of Twyman–Green interferogram between two aberrated wavefronts", Opt. Optoelect., 10(6) (2010) 553-556.
[33] R. Ghosh et al., "Twyman–Green interferometer of two propagating wavefronts with optical aberration", J. Opt. Design, 6(4) (2016) 367-372.
[34] E. Recupero et al., "determination of optical path difference in two interferograms with mutually shear perpendicular directions", J. Opt. Technol., 16(2) (2020) 87-92.
[35] K. Chandra Pati et al., "Numerical analysis of optical path difference of two perpendicular", Opt. Commun., 20(8) (2012) 805-810.
[36] S. Mukhija et al., "Optical path difference between two interferograms consisting of mutual perpendicular shear directions", J. Laser Technol., 13(11) (2012) 1543-1550.
[37] U. Vianney et al., "Fourier filtering of optical path difference between two interferograms", Opt. Phys. Lett., 15(6) (2015) 313-320.
[38] A. Sergyienko et al., "Analysis of optical path difference in interferometer using least-squares method", Opt. Phys. Lett., 16(5) (2016) 535-540.
[39] O.A. Hamadi and K.Z. Yahiya, "Optical and electrical properties of selenium-antimony heterojunction formed on silicon substrate", J. Pure Appl. Sci., Univ. Sharjah, 4(2) (2007) 1-11.
[40] D. Carter et al., "Analysis of mutual perpendicular shear directions for propagating wavefronts using least-squares method", J. Opt. Design, 10(6) (2020) 483-488.
[41] R. White et al., "Estimation of optical path difference in two-zone-plates interferogram using least-squares method", J. Opt. Technol., 11(3) (2015) 303-310.
[42] X. Zhang et al., "Multi-directional optical path difference due to shearing wavefront", Opt. Commun., 22(6) (2014) 633-638.
[43] J. Rogers et al., "Radial shear analysis of Twyman–Green free-aberration interferometer", J. Laser Technol., 14(12) (2013) 1-10.
[44] C. Gejdenson et al., "Design considerations of low-aberration Twyman–Green interferometer with radially sheared wavefronts", J. Opt. Phot., 6(12) (2016) 1143-1148.

 ISSN (print) 2958-8960 (online) xxxx-xxxx Printed in IRAQ